ARTICLE

Trench-Parallel Flow Beneath the Nazca Plate from Seismic Anisotropy

R. M. Russo and P. G. Silver

Shear-wave splitting of *S* and *SKS* phases reveals the anisotropy and strain field of the mantle beneath the subducting Nazca plate, Cocos plate, and the Caribbean region. These observations can be used to test models of mantle flow. Two-dimensional entrained mantle flow beneath the subducting Nazca slab is not consistent with the data. Rather, there is evidence for horizontal trench-parallel flow in the mantle beneath the Nazca plate along much of the Andean subduction zone. Trench-parallel flow is attributable to retrograde motion of the slab, the decoupling of the slab and underlying mantle, and a partial barrier to flow at depth, resulting in lateral mantle flow beneath the slab. Such flow facilitates the transfer of material from the shrinking mantle reservoir beneath the Pacific basin to the growing mantle reservoir beneath the Atlantic basin. Trench-parallel flow may explain the eastward motions of the Caribbean and Scotia sea plates, the anomalously shallow bathymetry of the eastern Nazca plate, the long-wavelength geoid high over western South America, and it may contribute to the high elevation and intense deformation of the central Andes.

One of the most important implications of the plate tectonic revolution is that the mantle is convecting; yet progress in the characterization of mantle flow over the subsequent decades has been slow. The principal obstacle to the determination of the actual mantle flow regime is that observational constraints are few. Our most direct indicators of mantle flow are the motions of the surface plates and, secondarily, the positions, motions, and ultimate fate of subducted slabs (*1–9*). However, the use of plate and subducted-slab characteristics to deduce mantle flow entails all-important assumptions regarding the coupling of slab and mantle.

Recently, it has become possible to make use of a direct, high-resolution measure of upper mantle flow: shear-wave splitting resulting from deformation-induced seismic anisotropy (*10–18*). Observations of shear-wave splitting, and hence of mantle flow, are limited only by the geometry of the global distribution of earthquakes and seismometers, and therefore represent a little-exploited global data set having immediate potential for the testing of mantle flow models. In particular, we can test the long-held assumption that mantle flow beneath subducting oceanic lithosphere is strongly coupled to and entrained by slab motion (*19, 20*).

The conventional model of mantle flow in the vicinity of subduction zones posits that this flow is predominantly two-dimensional (Fig. 1). The flow trajectory of material in the mantle wedge overlying the slab is governed by the relative plate motion (RPM) between the subducting and overriding plates, and the flow in the mantle below the slab is presumed to be largely coupled to the slab, or entrained, and to mimic the slab motion as it subducts. Mantle flow beneath the slab would therefore parallel the direction of absolute plate motion (APM) of the subducting plate. It is also generally assumed that the oceanic plates move relative to the deep mantle along a decoupling zone, the asthenosphere. But the thickness of this zone, the degree of decoupling it represents, the variability of motions it might encompass, and whether it survives the subduction process remain poorly known.

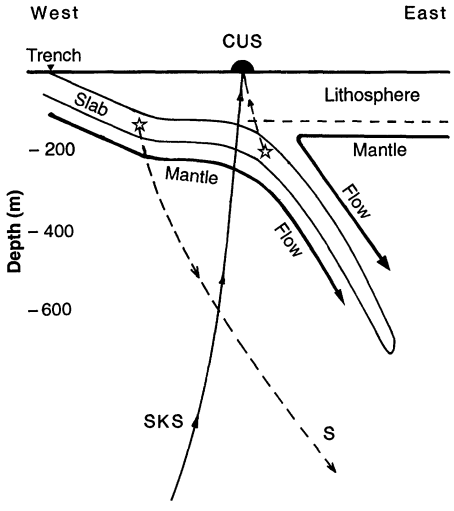

Fig. 1. Schematic section of the subducted Nazca plate at 14°S [after (*30*)]. The conventional flow model is based on the assumption of two-dimensional flow above (corner flow) and below (progressive simple shear in thin layer) the slab. Trajectories of various *S* waves are shown. *SKS* from teleseismic events samples both above and below the slab. *S* waves from events directly below the station sample the region above the slab. In combination, they can be used to isolate contributions from above and below the slab. Direct *S* waves (dashed trajectory) recorded teleseismically sample primarily below slab.

Shear-wave splitting data from broadband digital stations can be used to measure directions of mantle flow in the vicinity of subducting slabs. We present splitting measurements for the Andean subduction zone and adjoining regions. This subduction zone is ideal for our purposes in that it is highly active seismically along its 7000-km length; the continent overlies the slab, providing ample opportunity for the strategic placement of seismometers; the convergence direction between the subducting Nazca plate and continental South America (RPM) admits little obliquity (*21, 22*); and the APM directions of the two plates are virtually parallel to the RPM direction. Therefore, we expect mantle flow in the vicinity of this slab to be relatively simple and predominantly two-dimensional, as in the slab-entrained flow model described above.

Measuring Shear-Wave Splitting and Seismic Anisotropy

The primary mineral constituent of the upper mantle, olivine, is elastically anisotropic and develops a definite fabric (referred to as lattice-preferred orientation, or LPO) in response to even modest finite strain (*10, 15, 23–27*). The deformation of olivine at upper-mantle pressures and temperatures results in the predominant alignment of *a* axes [100] of single olivine crystals in an aggregate within the flow plane and along the flow line (*28*). The seismic anisotropy resulting from LPO in a peridotite aggregate of about 70% olivine probably averages about 3 to 6% for shear waves (*27, 29*). Thus, regions of the upper mantle in the olivine stability field, down to a depth of about 400 km that are subject to coherent deformation should be seismically anisotropic. Shear waves passing through such an anisotropic aggregate will split into fast and slow waves analogous to the bire-

The authors are in the Department of Terrestrial Magnetism, Carnegie Institution of Washington, 5241 Broad Branch Road, NW, Washington, DC 20015, USA.

fringence of light traversing an optically anisotropic medium. The properties of split shear waves (fast polarization direction, ϕ, delay time, δt) can then provide information such as the direction of flow and some constraint on the depth extent of the flowing region.

We used shear-wave splitting observed in two teleseismic phases, *S* and *SKS*, to achieve some measure of vertical resolution of anisotropic mantle masses near the subducted Nazca slab. Thus (Fig. 1), a combination of teleseismic *S* waves recorded at distant stations away from the subduction zone, upwardly propagating *S* waves recorded at seismometers in South America above the slab (*30*), and teleseismic *SKS* waves recorded at the South American stations allows us to isolate anisotropic regions above and below the slab and to assess correctly their contributions to the observed splitting. We use broad-band data because splitting is prominent on these seismograms, resolution is better than long period data, and the separation of seismic phases is facilitated. The direct *S* phases generated by events in the Nazca slab were recorded at seismographs in eastern South America, Africa, and North America (Fig. 2A). We used *SKS* phases from earthquakes worldwide to characterize the local splitting parameters at these stations (*16*) and then corrected the South American teleseismic *S* records to remove the local anisotropy contribution (*31–32*). The *S* waves from the South American slab to these stations sample the region beneath the slab almost exclusively (Fig. 1). The lateral resolution of shear-wave splitting measurements is excellent, on the order of 50 km, determined primarily by the Fresnel zone of the shear waves used.

SKS measurements. The *SKS* measurements (Fig. 2A and Table 1) comprise two groups. The first group is measurements we use to examine mantle anisotropy in the Andean subduction zone and adjoining areas. These include measurements for four

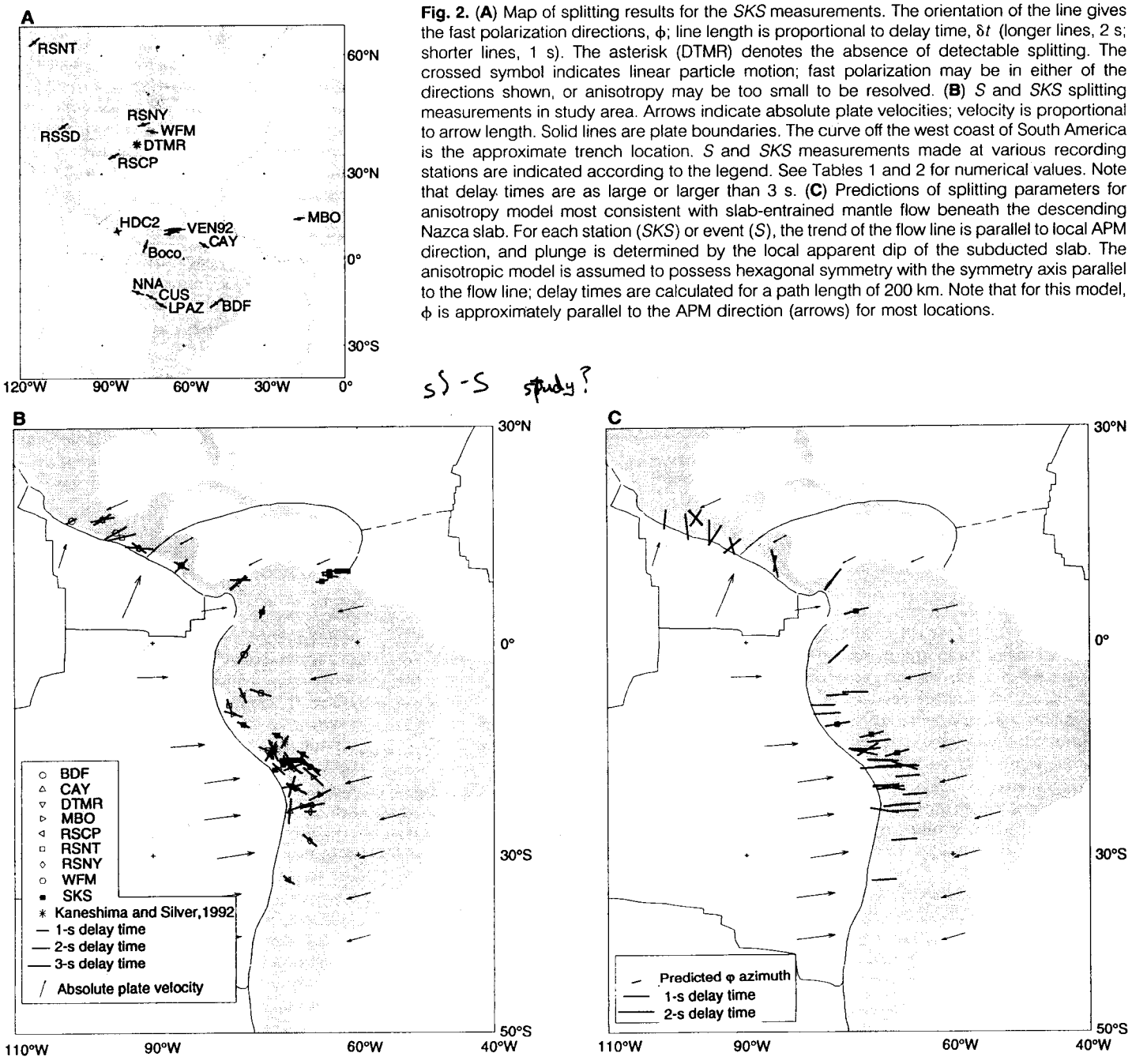

Fig. 2. (**A**) Map of splitting results for the *SKS* measurements. The orientation of the line gives the fast polarization directions, ϕ; line length is proportional to delay time, δt (longer lines, 2 s; shorter lines, 1 s). The asterisk (DTMR) denotes the absence of detectable splitting. The crossed symbol indicates linear particle motion; fast polarization may be in either of the directions shown, or anisotropy may be too small to be resolved. (**B**) *S* and *SKS* splitting measurements in study area. Arrows indicate absolute plate velocities; velocity is proportional to arrow length. Solid lines are plate boundaries. The curve off the west coast of South America is the approximate trench location. *S* and *SKS* measurements made at various recording stations are indicated according to the legend. See Tables 1 and 2 for numerical values. Note that delay times are as large or larger than 3 s. (**C**) Predictions of splitting parameters for anisotropy model most consistent with slab-entrained mantle flow beneath the descending Nazca slab. For each station (*SKS*) or event (*S*), the trend of the flow line is parallel to local APM direction, and plunge is determined by the local apparent dip of the subducted slab. The anisotropic model is assumed to possess hexagonal symmetry with the symmetry axis parallel to the flow line; delay times are calculated for a path length of 200 km. Note that for this model, ϕ is approximately parallel to the APM direction (arrows) for most locations.

stations located above the subducting Nazca plate: NNA (36), CUS (31), BOCO (32a), and LPAZ; one station near the middle America trench, HDC2; and portable stations in Venezuela (37) that sample the South American–Caribbean boundary. Although the *SKS* phases sample anisotropy both above and below the Nazca slab, in conjunction with upgoing *S* waves from slab events, we can isolate the anisotropy contribution in the mantle above the slab. The splitting in these upgoing waves has been measured for station CUS (30), for a network of portable stations between NNA and CUS in Peru (30), and for a network of portable stations in Colombia (38) just north of BOCO. At CUS, the delay times for the above-slab mantle path (Fig. 1) were approximately 0.1 s, whereas δt for *SKS* at CUS was 0.8 s (Table 1). Thus, most of the δt for this station is produced by anisotropy below the slab. For the Colombian and Peruvian portable stations, delay times for split upgoing *S* phases to these stations were typically 0.1 s and sometimes as great as 0.4 s (30, 38). Again, we infer that anisotropy above the slab is not well developed. Although we cannot rule out significant contributions to observed anisotropy at NNA or LPAZ, by analogy with CUS and the portable network results, we conclude that the primary source of splitting is in the mantle below the Nazca slab (39). With the limited number of events available to us, we could not confirm the presence of shear-wave splitting at station HDC2 (40), but the records we examined appeared to show no splitting. Finally, the portable stations in Venezuela yield the largest *SKS* delay times yet measured in South America, approaching 2 s (37). Splitting fast polarizations trend generally east-west (EW) for these stations.

The second group of stations (Fig. 2A) comprises those that we used to make measurements of splitting in teleseismic direct *S* waves resulting from anisotropy in the vicinity of the Nazca slab and adjoining areas. We characterized the local anisotropy at the stations (Table 1) to remove its contribution to observed splitting in direct *S* phases from our study area. All stations in this group exhibit splitting, with the exception of DTMR.

S measurements. Teleseismic *S* recorded at the distant stations of group 2, above, is a prominent and well-isolated phase for events deep enough to separate it from the surface reflections (depth > 40 km) and for the distance range of 30° to 80°, and thus we obtained a large number of observations of split direct *S* shear waves [see also (18)]. The contribution to splitting from anisotropy local to the receiver was removed from the records as mentioned above, and the resulting direct *S* splitting parameters were corrected for projection about the radial direction suffered during the transition from downward to upward travel from source to receiver. The records should thus accurately represent the splitting properties of the earthquake source region.

We examined nearly 350 broad-band records from several stations for which the measurement of direct *S* splitting parameters has been attempted (Fig. 2B and Table 2). Of the 105 records for which well-constrained splitting characteristics could be obtained, 43 yielded splitting parameters, and 62 records clearly exhibited linear particle motion, indicative of the absence of splitting. The latter signify that either the initial shear-wave polarization direction corresponds to the fast or slow polarization direction or that δt is less than about 0.5 s. Given the magnitudes of the delay times we constrain, it seems likely that the absence of splitting is a result of initial shear-wave polarization in most cases.

The combined *S* and South American *SKS* results are shown in Fig. 2B. The *S* measurement delay times range from 0.75 s to almost 4 s. Many measurements with large delay times lie in the region from 15° to 25°S; these values are the largest yet measured, globally. Also shown are data for events of the Middle Americas subduction zone and stations in the Caribbean basin. Delay times here are between 1 and 3 s. In both regions, fast polarization directions exhibit a complex pattern that we discuss further below.

Comparison to Conventional Model and Data Pattern

To compare our splitting observations with those predicted by the two-dimensional slab-entrained flow model, we calculated the anisotropic properties for such a model. We assumed that the trend of the flow line (Fig. 1) is parallel to the local APM direction and that its plunge is given by the local apparent dip of the Nazca plate along this trend. We assumed that the elastic properties of the medium have hexagonal symmetry, invoking the single crystal constants of olivine symmetrized to produce a hexagonally symmetric tensor with the *a* axis corresponding to the symmetry axis as in (11). We further assumed that the symmetry axis is parallel to the flow line, consistent with the behavior of olivine during coherent deformation outlined above. Finally, in specifying the geometry of the specific phase of interest, we assumed that for teleseismic *S* phases, the ray leaves the event and samples the source region at an angle equal to the takeoff angle predicted by the Earth model PREM (41) and along the source-receiver great circle azimuth. For *SKS* observations, we assume that the phase enters the anisotropic region beneath the receiver at near-vertical incidence. For the *S* phases, the predicted splitting parameters (Fig. 2C) are projected back to the location of the event as is done for the data. Delay times are computed for a 200-km-long path length in an anisotropic layer directly beneath the slab. The predictions should thus be directly comparable to the data.

Almost all the predicted ϕ values (Fig. 2C) for the Nazca and Cocos plates are roughly parallel to the local APM direction (42). Even a cursory comparison of the observed (Fig. 2B) and predicted ϕ values (Fig. 2C) reveals that the data bear little resemblance to this simple pattern. Rather,

Table 1. Station splitting parameters. Dashes indicate that no splitting was observed.

Station code	Station name	Latitude (degrees)	West longitude (degrees)	ϕ (degrees)	δt (s)	Reference
BARV	Barcelona, Ven92	10.670	63.000	94	1.4	*37*
BDF	Brasilia	−15.664	47.903	53	1.5	*
BOCO	Bogota	4.590	74.040	20	1.2	*59*
CAY	Cayenne	4.948	52.317	119	0.7	*
CECV	Cerro El Canito, Ven92	10.570	64.170	81	1.9	*37*
CUS	Cuzco	−13.563	71.877	115	0.8	*30*
DTMR	DTM-Carnegie	38.960	77.060	—	—	*59*
ECPV	El Chaparro, Ven92	9.180	65.250	79	0.7	*37*
HDC2	Heredia	10.270	84.117	—	—	*
LPAZ	La Paz	−16.288	68.131	120	1.1	*
MBO	M'Bour	14.391	16.955	82	0.7	*
MNVV	Mundo Nuevo, Ven92	9.950	64.030	101	1.3	*37*
NNA	Nana	−11.988	76.842	113	1.2	*31, 36*
RSCP	Cumberland	35.590	85.570	59	0.7	*16*
RSLV	Rio Salado, Ven92	10.650	62.250	89	1.6	*37*
RSSD	Black Hills	44.120	104.040	55	0.6	*16*
RSNT	Yellow Knife	62.480	114.590	51	1.2	*16*
RSNY	Adirondack	44.550	74.530	74	0.9	*16*
WFM	Westford	42.610	71.490	100	0.8	*60*

*This study.

they are much more complex and indicate that the actual flow-induced anisotropy is highly variable, whereas the expected distribution of anisotropy is rather uniform. We must conclude on this basis that the slab-entrained flow model fails to provide an adequate explanation for these data. Despite the complex pattern, however, the measured splitting directions display systematic variations relative to the local strike of the nearest subduction trench. For the Andean subduction zone (Fig. 3, A and B), two populations of measurements are visible (*43*): 17 that are locally parallel (less than 30°) to the trench and 11 that are more nearly trench-normal (greater than 60°), sometimes nearer the APM direction (eight fall in neither group). All but two of the trench-normal group are localized in three narrow (200 km) geographic zones (Fig. 3A). The northernmost of these zones is also at a very high angle to the APM-predicted splitting directions.

Excluding these three zones, the predominantly trench-parallel ϕ observations lead us to conclude that mantle flow beneath much of the Nazca slab includes a significant component of trench-parallel flow (*44*). The large delay times we observe allow us to rule out the possibility that this flow is restricted to a very thin layer beneath the slab: The observed degree of anisotropy in olivine aggregates requires a zone on the order of 100 to 200 km in thickness to produce these delay times. Thus, this flow represents a large volume of subslab mantle in motion relative to the slab itself. At the Middle Americas subduction zone, the observed ϕ directions are not consistent with the ϕ directions predicted on the basis of the APM model of the Cocos plate. However, more data are necessary to describe this region adequately. Finally, we note that the pattern of mantle flow we observe beneath the Nazca plate is consistent with observations of azimuthal anisotropy in long-period Rayleigh waves (*45*).

A Physical Model Consistent with Trench-Parallel Flow

It is difficult to see how a component of trench-parallel flow could be present beneath the Nazca slab without violating the essential assumptions of the slab-entrained flow model. Nothing in the motions of these two plates in the absolute or relative frames would lead us to expect this type of flow, if the subslab mantle moves coherently with the slab. If flow is constrained to move parallel to the slab surface, then any three-dimensional flow includes a component of trench-parallel motion. Three-dimensional mantle flow directly beneath the slab principally violates the assumption that some significant width of subslab mantle

Table 2. *S* splitting measurements (receiver corrected). The standard errors of ϕ (σ_ϕ) and of δt ($\sigma_{\delta t}$) are given.

Station code	Date	Time (UT)	Latitude (degrees)	West longitude (degrees)	Depth (km)	ϕ (degrees)	σ_ϕ (degrees)	δt (s)	$\sigma_{\delta t}$ (s)
RSSD	15 Sep 1982	20:22:55.3	−14.500	70.800	176	30	18	1.2	0.7
BDF	18 Nov 1982	14:57:52.4	−1.719	76.703	195	33	24	2.8	0.9
BDF	24 Jan 1983	08:17:39.6	16.147	95.232	57	60	11	3.3	0.6
RSNY	25 Feb 1983	22:49:54.7	−18.268	69.438	146	124	11	2.3	0.5
RSNY	01 Sep 1983	20:01:47.1	−17.330	69.932	105	145	11	2.9	0.5
RSNY	02 Dec 1983	03:09:05.7	14.053	91.940	68	126	11	1.9	0.9
RSNT	02 Dec 1983	03:09:05.7	14.053	91.940	68	95	11	3.8	0.6
RSCP	15 Dec 1983	04:22:28.5	−33.091	70.278	54	128	12	1.3	0.6
RSCP	26 Feb 1984	08:18:16.7	−17.264	70.572	85	106	11	1.1	0.5
RSNY	26 Feb 1984	08:18:16.7	−17.264	70.572	85	155	11	2.7	0.5
RSCP	05 Jun 1984	04:15:24.8	−7.765	76.863	36	155	16	1.7	0.6
RSNT	18 Jun 1984	11:20:18.3	−15.725	72.478	121	157	11	3.1	0.8
RSSD	18 Jun 1984	11:20:18.3	−15.700	72.500	121	25	18	1.5	0.7
RSNY	20 Oct 1984	17:59:18.8	−24.264	67.064	212	90	11	0.8	0.7
RSNY	20 Apr 1985	18:23:48.3	8.979	77.527	40	46	12	2.7	0.6
RSNY	10 Jun 1985	15:37:03.4	−28.112	67.185	180	130	11	2.1	0.6
RSNT	21 Aug 1985	11:26:28.8	−9.211	78.908	61	161	13	1.2	0.7
RSNT	15 Sep 1985	07:57:53.8	17.975	97.183	67	79	14	3.1	0.8
RSNY	15 Sep 1985	07:57:53.8	17.975	97.183	67	57	12	2.4	0.8
BDF	21 Sep 1985	01:37:13.8	17.823	101.670	33	62	16	0.8	0.5
RSNT	07 Apr 1986	22:43:31.2	15.551	94.385	61	70	16	4.0	0.9
CAY	06 Mar 1987	09:39:54.3	−24.204	70.073	45	6	11	3.6	0.6
MBO	25 Jan 1988	07:15:53.5	−10.450	78.320	73	108	19	2.2	0.6
CAY	06 Feb 1988	18:03:53.6	−18.030	67.020	285	126	21	2.5	0.9
MBO	06 Feb 1988	18:03:53.6	−18.030	67.020	285	135	12	3.5	0.6
WFM	06 Feb 1988	18:03:53.6	−18.030	67.030	285	113	15	2.6	0.6
MBO	22 Feb 1988	19:13:17.7	−20.833	69.785	70	17	11	2.7	0.6
WFM	22 Feb 1988	19:13:17.4	−20.530	69.570	67	81	11	2.6	0.5
CAY	06 May 1988	14:46:18.0	11.520	85.800	76	43	22	2.0	0.7
WFM	06 May 1988	14:46:18.0	11.520	85.800	76	119	14	1.7	0.5
MBO	04 Jul 1988	13:54:16.0	−18.350	71.720	27	135	12	1.9	0.5
MBO	28 Jul 1988	17:12:32.8	−22.010	65.610	295	64	11	3.1	0.5
MBO	14 Sep 1988	22:14:07.7	−23.500	68.240	140	72	11	3.2	0.5
WFM	29 Nov 1989	01:00:15.3	−15.680	73.310	66	113	16	2.2	0.8
WFM	03 Dec 1989	14:16:48.8	−7.370	74.270	151	107	12	2.8	0.8
MBO	24 Dec 1988	04:26:57.0	−23.430	66.700	218	80	11	3.1	0.5
CAY	06 Apr 1989	23:47:50.5	−21.130	69.090	122	115	22	2.8	0.8
MBO	06 Apr 1989	23:47:50.5	−21.130	69.090	122	119	22	3.1	0.8
CAY	04 Apr 1990	05:47:10.5	−16.179	72.974	93	32	16	1.9	0.6
MBO	17 May 1990	11:03:24.8	−18.080	69.626	105	69	16	2.4	0.8
MBO	10 Oct 1990	01:00:05.5	−19.503	66.618	266	134	17	4.0	0.8
MBO	04 Nov 1990	18:13:43.1	−15.721	72.619	121	175	27	2.2	1.0
DTMR	20 Apr 1991	07:01:57.2	9.392	77.281	36	89	11	2.5	0.6

(asthenosphere) is strongly coupled to and therefore entrained by the descending plate. If this assumption is incorrect, then subducted lithosphere must be largely decoupled from underlying asthenosphere. Rather, the slab serves primarily as a bounding surface between the subslab Pacific mantle on one side and the South American subcontinental mantle on the other, modulating subslab mantle flow by transmitting stresses normal to its surface. The idea that the Nazca slab is decoupled from its underlying asthenospheric mantle is the basis for the remainder of our discussion. If our postulate is correct, then we must examine the specific features of the Nazca slab, its motions in the absolute frame, and its shape, primarily, that might most profoundly affect the response of the mantle it overlies. We also consider the effects of the pressure gradients associated with flow in the subslab mantle on the regional geoid and on the tectonics of the study area.

The retrograde flow hypothesis. If the slab is effectively decoupled from the mantle below, then its primary influence on mantle flow is due to slab motions normal to the slab surface. This motion could move the slab toward or away from the overriding plate. In fact, the Nazca trench moves westward, away from overriding South America, although the two plates converge (*21, 22*). This type of slab motion has been referred to as retrograde motion (*2, 8, 9, 46, 47*). The models of this flow depend on many factors, but it is clear that subslab mantle flow induced by slab retrograde motion is generally three-dimensional and may have components in the trench-parallel direction. Thus, mantle material could pass laterally around a slab that is not infinite in along-strike extent, as well as below the end of a slab that does not extend infinitely down-dip (*8, 9*). Furthermore, barriers to flow in the trench-parallel direction or to flow beneath the slab also modulate subslab flow. In the first case, flow would be forced below the end of the slab; a barrier to flow beneath the end of the slab would force flow laterally in the trench-parallel direction. Hence, retrograde flow could induce the trench-parallel flow component we infer in the sub-Nazca slab mantle (Fig. 4A). If this effect is true for the 7000 km length of the South American subduction zone, then we relate trench-parallel splitting measurements in northern South America to northward trench-parallel flow (toward the nearest slab truncation) along the northern half of the Andean subduction zone. Likewise, southward trench-parallel flow in the southern half of the subduction zone would give rise to trench-parallel values of ϕ in this region. We might also expect a stagnation point with little or no trench-parallel flow (but with maximum pressure) between these two areas (Fig. 4, A and B).

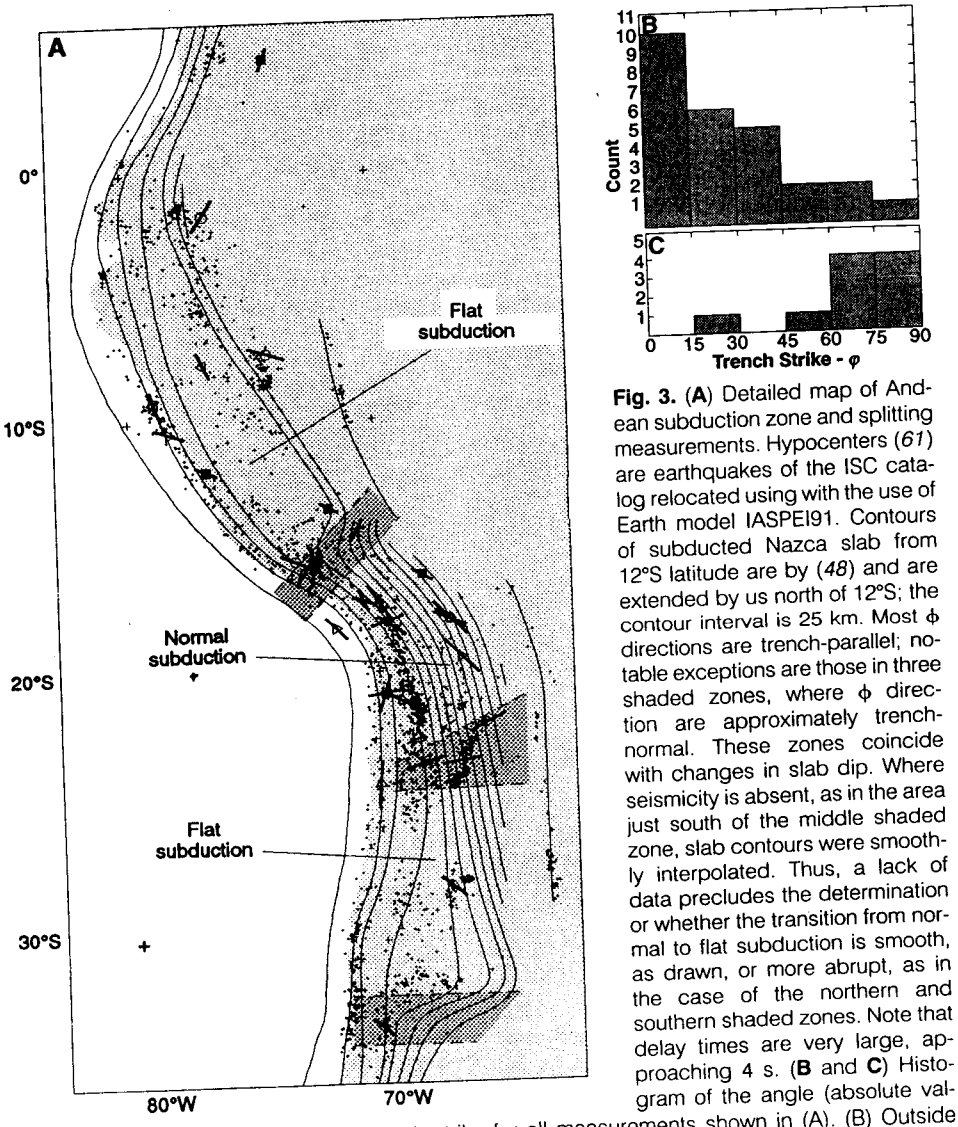

Fig. 3. (**A**) Detailed map of Andean subduction zone and splitting measurements. Hypocenters (*61*) are earthquakes of the ISC catalog relocated using with the use of Earth model IASPEI91. Contours of subducted Nazca slab from 12°S latitude are by (*48*) and are extended by us north of 12°S; the contour interval is 25 km. Most ϕ directions are trench-parallel; notable exceptions are those in three shaded zones, where ϕ direction are approximately trench-normal. These zones coincide with changes in slab dip. Where seismicity is absent, as in the area just south of the middle shaded zone, slab contours were smoothly interpolated. Thus, a lack of data precludes the determination or whether the transition from normal to flat subduction is smooth, as drawn, or more abrupt, as in the case of the northern and southern shaded zones. Note that delay times are very large, approaching 4 s. (**B** and **C**) Histogram of the angle (absolute value) between ϕ direction and local trench strike for all measurements shown in (A). (B) Outside shaded zones. (C) Within shaded zones. Note that measurements outside the zones are predominantly trench-parallel; those within shaded zones are trench-normal.

Our hypothesis does not account for the zones of trench-normal measurements (Figs. 3A and 4B). We suggest that in addition to retrograde slab motion, slab morphology may locally have an effect on flow induced in a decoupled subslab asthenosphere. For example, abrupt changes in the dip of the slab might result in localized pressure gradients in the mantle and perhaps perturbations in the mantle flow field. A tear in the slab would almost certainly have a strong effect on the mantle flow field near the tear, because it would represent a direct conduit for the transfer of mantle from one side of the slab to the other. We infer that slab morphology may be related to this group of splitting measurements: The northernmost of these zones is the site of a well-documented abrupt along-strike change in slab dip from flat subduction in the north to normal subduction in the south (*31, 48, 49*). The central zone appears to correspond to an equivalent transition from normal back to flat subduction, although the abrupt diminution of seismicity at this latitude renders this a more difficult transition to resolve. The southern zone represents a transition back to normal subduction (*48*).

Consequences of retrograde flow. Important consequences of retrograde trench-parallel flow may include the dynamic support of topography and corresponding geoid anomalies, given the lateral pressure gradient required to drive the flow. We can assess this effect by means of a simple calculation. Assuming the trench-parallel flow is analogous to simple channel flow, one can express the average flow velocity $\bar{u}$ as

$$\bar{u} = -\frac{l^2}{12\mu} dp/dx$$

(*50*) where μ is the viscosity, l is the width of the channel, and dp/dx is the pressure gradient. We further assume that dp/dx can be directly related to uplift, h, ($dp/dx = \rho gh/D$, where g is gravitational acceleration, D is the length, 3500 km, from the stagnation point to the tip of South America, and ρ is the mantle density for continental regions or the difference between mantle and seawater density for oceanic regions). If $\mu = 10^{19}$ Pa·s and $l = 200$ km, then for the ocean (continent) 150 (100) m of uplift is produced for every 1 cm per year of trench-parallel flow. Thus, an elevation change of about 0.75 (0.50) km corresponds to 5 cm/year of horizontal flow. The expected geoid anomaly for 0.5 km of dynamic topography is on the order of 10 to 20 m, with the assumption of a compensation depth of 200 to 300 km. Thus, we might expect a 20-m geoid high situated in the middle of the South American subduction zone, compared to the northern and southern tips. The observed geoid (Fig. 5) includes a 30-m height differential between the center of South America and its northern and southern tips. The geoid high coincides with the most elevated region of the Andes and also extends over anomalously shallow Nazca bathymetry (*51*, *52*). The shallow Nazca bathymetry is important because it is not a consequence of deformation-induced crustal thickening, as is perhaps true of the Andean elevations. The pressure gradients associated with trench-parallel retrograde flow provide a plausible explanation for the South American geoid high and predict the correct sign and magnitude for variations in elevation. The long-wavelength component of this geoid anomaly has been attributed to the mass excess of the subducted slabs (*6*, *53*, *54*). However, models of the geoid based solely on the slab density anomaly predict a 1-km topographic depression (*54*) and anomalous subsidence, rather than uplift, over this region. This depression is not observed, and we conclude that the slab mass excess cannot be the only contribution to this long-wavelength geoid anomaly. Trench-parallel flow is consistent with the observed uplift of the Andes and the Nazca plate and therefore may be the dominant contribution to the geoid in this area.

Trench-parallel retrograde flow may also have important tectonic consequences. It is inferable from global plate motion models that not only the Andean subduction zone but all the subduction zones surrounding the Pacific basin are in retrograde motion (*2*, *8*, *46*). That is, in an absolute frame, they are moving toward the center of the Pacific basin, thus reducing its area. As a consequence, to conserve mass, mantle material must flow from the Pacific into the Atlantic and Indian basins. Some part of this transfer of mass from the sub-Pacific mantle reservoir to the sub-Atlantic mantle reservoir may be reflected in the eastward motion of the Caribbean and the Scotia Sea plates (Fig. 4B) (*46*). Our splitting measurements [including *SKS* measurements along the eastern Caribbean–South American plate boundary zone characterized by very large delay times (2 s) and EW ϕ directions (*37*)] in conjunction with the retrograde flow hypothesis, lend credence to this idea.

Secondly, trench-parallel retrograde flow may account in part for the character of deformation in the overriding South American continent. The westward motion of South America in an absolute frame can be viewed as the movement of the continent (mediated by the Nazca plate) through a viscous fluid. Then the maximum in pressure applied to the leading edge of the continent occurs at the stagnation point (*55*) with a corresponding maximum in deformation. We note that the greatest horizontal shortening in the Andes is located in the central Andes (*56*), above the proposed location of the mantle flow stagnation point.

Finally, the existence of trench-parallel retrograde flow implies that the subslab mantle encounters a barrier to flow that prevents it from moving in the down-dip

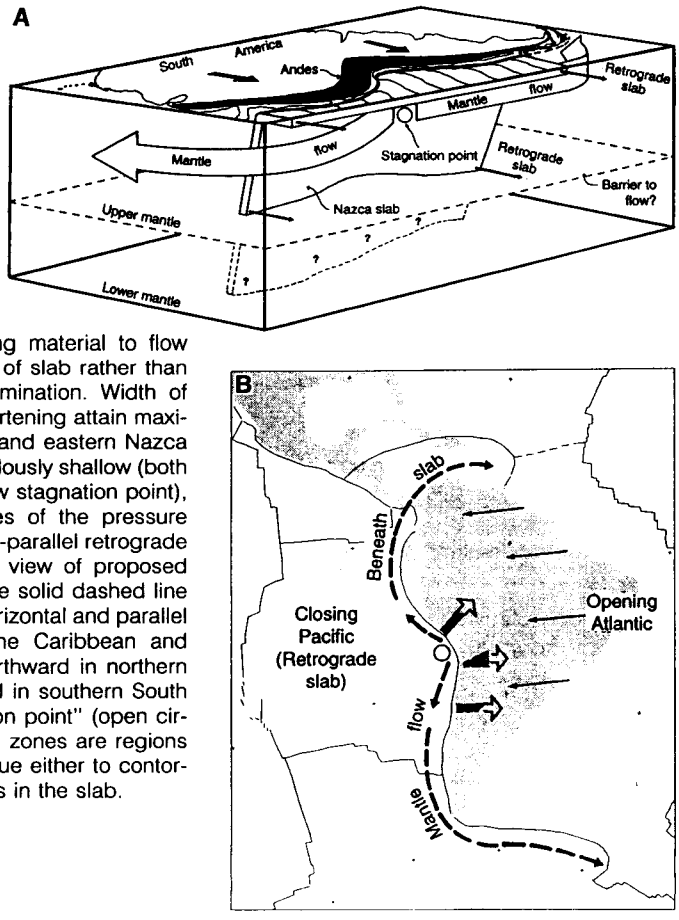

Fig. 4. (**A**) Schematic block view of proposed retrograde flow. The coupling between downgoing slab and underlying mantle is weak, and mantle just below slab flows laterally as a consequence of pressure induced by retrograde motion of slab. We hypothesize that mantle below slab encounters a barrier at depth, forcing material to flow around lateral truncations of slab rather than beneath its down-dip termination. Width of orogen and horizontal shortening attain maxima in the central Andes, and eastern Nazca plate bathymetry is anomalously shallow (both coincident with mantle flow stagnation point), perhaps as consequences of the pressure gradient that drives trench-parallel retrograde flow. (**B**) Schematic map view of proposed retrograde flow model. The solid dashed line is the plan view of flow, horizontal and parallel to coast, passing into the Caribbean and Scotia basins. Flow is northward in northern South America, southward in southern South America, with a "stagnation point" (open circle) in the center. Shaded zones are regions of locally disrupted flow due either to contortions or to actual breaches in the slab.

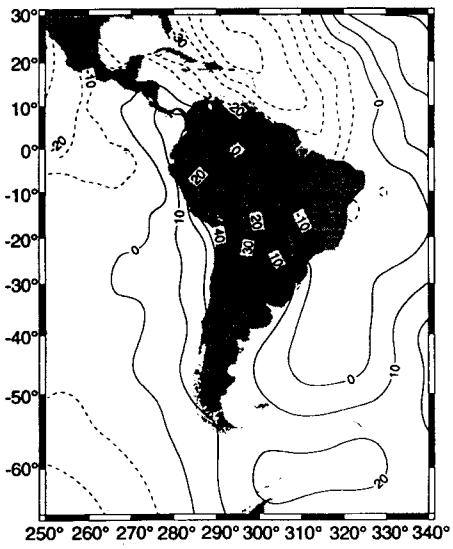

Fig. 5. Geoid anomaly map of the South American region (*62*, *63*). Heights are given in meters, and the contour interval is 10 m. Note the 40-m geoid high in the center of South America that decreases to near 0 m at the northern and southern ends of the continent. We associate this change with dynamically supported topography resulting from a pressure gradient required to drive lateral retrograde flow.

direction and into the lower mantle beneath South America. Thus, even if the Nazca slab penetrates into the lower mantle (*57*), the subslab mantle does not. A barrier to upper and lower mantle mixing is not consistent with unrestrained whole mantle flow. Rather, the decoupling of slab and mantle and the inability of nonslab upper mantle to flow into the lower mantle suggest a penetrative convection-flow regime (*58*).

REFERENCES AND NOTES

1. H. Hess, *Nature* **203**, 629 (1962).
2. W. M. Elsasser, *J. Geophys. Res.* **76**, 1101 (1971).
3. T. H. Jordan, *J. Geophys.* **43**, 473 (1977).
4. F. M. Richter, *J. Geophys. Res.* **84**, 6783 (1979).
5. K. C. Creager and T. Jordan, *ibid.* **89**, 3031 (1984); K. C. Creager and T. Jordan, *ibid.* **91**, 3573 (1986).
6. B. H. Hager, *ibid.* **89**, 6003 (1984).
7. P. Silver and W. Chan, *ibid.* **91**, 13787 (1986).
8. Z. Garfunkel, C. A. Anderson, G. Schubert, *ibid.*, p. 7205.
9. C. Kincaid and P. Olson, *ibid.* **92**, 13832 (1987).
10. N. I. Christensen, *ibid.* **71**, 5921 (1966).
11. C. M. Keith and S. Crampin, *Geophys. J. R. Astron. Soc.* **49**, 225 (1977).
12. M. Ando, *J. Phys. Earth* **32**, 179 (1984).
13. Y. Fukao, *Nature* **309**, 695 (1984).
14. L. P. Vinnik, V. Farra, B. Romanowicz, *Bull. Seismol. Soc. Am.* **79**, 1542 (1989).
15. N. M. Ribe, *J. Geophys. Res.* **94**, 4213 (1989).
16. P. G. Silver and W. W. Chan, *ibid.* **96**, 16429 (1991); see also P. Silver and W. Chan, *Nature* **335**, 34 (1988).
17. M. K. Savage and P. G. Silver, *Phys. Earth Planet Inter.* **78**, 207 (1993).
18. L. P. Vinnik and R. Kind, *Geophys. J. Int.* **113**, 165 (1993).
19. D. L. Turcotte and E. R. Oxburgh, *Phys. Today* **22**, 30 (1969).
20. D. P. McKenzie, *Sci. Am.* **249**, 67 (September 1983).
21. C. DeMets *et al.*, *Geophys. J. Int.* **101**, 425 (1990).
22. A. E. Gripp and R. G. Gordon, *Geophys. Res. Lett.* **17**, 1109 (1990).
23. T. Francis, *Nature* **221**, 162 (1969).
24. M. Kumazawa and D. L. Anderson, *J. Geophys. Res.* **74**, 5961 (1969).
25. A. Nicolas, F. Boudier, A. M. Boullier, *Am. J. Sci.* **273**, 853 (1973).
26. S. Karato, M. Toriumi, T. Fujii, *Geophys. Res. Lett.* **7**, 649 (1980).
27. D. Mainprice and P. G. Silver, *Phys. Earth Planet. Inter.* **78**, 257 (1993).
28. A. Nicolas and N. I. Christensen, in *Composition, Structure, and Dynamics of the Lithosphere-Asthenosphere System*, K. Fuchs and C. Froidevaux, Eds. (American Geophysical Union, Washington, DC, 1987).
29. N. I. Christensen, *Geophys. J. R. Astron. Soc.* **76**, 89 (1984).
30. S. Kaneshima and P. G. Silver, *Phys. Earth Planet. Inter.*, in press.
31. S. Kaneshima and P. G. Silver, *Geophys. Res. Lett.* **19**, 1049 (1992).
32. In using *SKS* receiver-splitting parameters to correct the *S* arrivals for receiver structure, we make the approximation that these parameters are not strong functions of arrival angle, because the arrival angles for *S* range from about 17° to 27°, versus about 10° for *SKS*. Based on calculations with various simple models of anisotropy, this approximation appears to hold, except that the delay times can in some cases be biased to higher values [see (*33*)]. However, if the observed receiver-splitting parameters of *S* and *SKS* are compared (*17, 30, 34, 35*), this bias appears to be small. In addition, the receiver splitting delay times are in most cases much smaller than the source delay times, further reducing errors.

32a. L. P. Vinnik, L. J. Makageva, A. Yu Usenko, *Geophys. J. Inter.* **111**, 433 (1992).
33. K. M. Fischer, *Eos* **74**, 403 (1993).
34. D. E. McNamara, T. J. Owens, P. G. Silver, F. T. Wu, *J. Geophys. Res.*, in press.
35. L. P. Vinnik, R. Kind, G. L. Kosarev, L. I. Makeyeva, *Geophys. J. Int.* **99**, 549 (1989).
36. G. Helffrich, P. G. Silver, H. Given, in preparation.
37. R. Russo, P. G. Silver, D. E. James, *Eos* **74**, 300 (1993).
38. X. R. Shih, J. F. Schneider, R. P. Meyer, *J. Geophys. Res.* **96**, 12069 (1991).
39. The contribution to observed anisotropy by the slab itself is probably negligible because the Nazca slab is relatively young [65 million years ago (Ma)] and therefore thin. For example, propagation along a 60-km path through a layer with 4% anisotropy, commensurate with the age and composition of the Nazca slab, yields only a 0.5-s delay time in the exiting split shear wave, much less that we observe. In addition, the expected form of anisotropy in the slab is inconsistent with the observations. We expect two possible directions: A fast direction consistent with (i) fossil anisotropy formed at the spreading center (parallel to fracture zones, NE-SW); or (ii) an EW fast direction associated with the more recent absolute motion of the plate. Thus, because the direction of (i) is nearly orthogonal to the observed ϕ directions, if we correct *SKS* splitting parameters for the slab contribution, we would tend to increase the delay times observed without significantly altering the observed ϕ. Case (ii) is indistinguishable from flow below the slab, so that it can be tested along with the APM model discussed below.
40. V. Ansel and H.-C. Nataf, *Geophys. Res. Lett.* **16**, 409 (1989).
41. A. M. Dziewonski and D. L. Anderson, *Phys. Earth Planet Int.* **25**, 297 (1981).
42. In some cases, the predicted value of ϕ is significantly different from the APM direction. This occurs when (i) slab dip and ray takeoff angle are nearly equal and (ii) the angle between the trend of symmetry axis and the ray azimuth is less than about 45°. In this case, the value of ϕ is relatively insensitive to, and thus only weakly constrains, the direction of the symmetry axis. This relation is seen for the most northern *S*-wave measurement in South America and several points along the Middle America trench, where the slab dips are the steepest.
43. Some data complexity is due to uncertainties in the measurement of ϕ. One such uncertainty is caused by noise on the seismogram, and the statistics of this effect are given in (*16*). An additional source of error, in the case of the *S* waves, is that introduced by errors in the receiver correction and in trade-offs between splitting parameters and the estimate of the initial polarization direction. On the basis of the results of (*31*), we combined the estimated uncertainty from the measurement procedure with those from other causes (the other errors have been given a nominal standard error of 10° for ϕ and 0.5 s for δt) by adding their variances. The error bars in Table 2 reflect this procedure. Some of the variation in splitting parameters may be due to the actual form of mantle anisotropy and may ultimately be used as additional diagnostics. For example, as is evident from Fig. 2B, the delay times from *SKS* are about half as large as for *S* on average. The APM model predicts delay times that are roughly comparable (Fig. 2C). In contrast, a model with the *a* axis horizontal and locally parallel to the trench, consistent with what we are proposing, does in fact predict significantly larger delay times for *S* compared to *SKS*.
44. Even if all of the measurements are taken together, the number of ϕ values in the trench-parallel (0° to 30°) direction is significantly greater than that expected by chance alone at the 94% confidence level.
45. J. P. Montagner and T. Tanimoto [*J. Geophys. Res.* **96**, 20337 (1991)] used surface waves to resolve azimuthal anisotropy globally. They found strong anisotropy associated with spreading ridges, with fast azimuthal direction (which should be parallel to the ϕ directions we measure, assuming hexagonal symmetry and a horizontal symmetry axis) parallel to the APM direction. For the Nazca plate, their fast direction rotates from EW (APM direction) near the East Pacific Rise to NS at the west coast of South America. This result is most visible for waves with periods of 250 s, which primarily sample the mantle beneath the plate. At a shorter period (100 s), sampling correspondingly shallower mantle, this rotation to NS is weaker; therefore, the anisotropic material sampled is probably primarily below the slab.
46. W. Alvarez, *J. Geophys. Res.* **87**, 6697 (1982).
47. B. H. Hager, R. J. O'Connell, A. Raefsky, *Tectonophysics* **99**, 165 (1983).
48. T. Cahill and B. Isacks, *J. Geophys. Res.* **97**, 17503 (1992).
49. A. Hasagawa and I. S. Sacks, *ibid.* **86**, 4971 (1981).
50. D. L. Turcotte and G. Schubert, *Geodynamics* (Wiley, New York, 1982); J. P. Morgan and W. H. F. Smith, *Nature* **359**, 524 (1992).
51. S. T. Crough, *Annu. Rev. Earth Planet. Sci.* **11**, 165 (1983).
52. J. C. Marty and A. Cazenave [*Earth Planet. Sci. Lett.* **94**, 301 (1989)] estimated the subsidence rate for 30 oceanic regions. They found that the Nazca plate has the lowest subsidence rate of any plate, 50 to 100 m/Ma$^{1/2}$ slower than the global average subsidence rate. With the global average as the "true" rate, the residual bathymetry for the oldest parts of the Nazca plate (about 65 Ma) close to the coast corresponds to 400 to 800 m of residual uplift. These authors note that imputing such large variations in subsidence rate to asthenospheric temperature variations is implausible, because a subsidence rate 100 m/Ma$^{1/2}$ lower than the average corresponds to a low asthenospheric temperature beneath the spreading ridge. We suggest that these low subsidence values are due to the pressure gradients associated with trench-parallel retrograde flow. The values of residual bathymetry are of the same sign and roughly consistent in magnitude with those expected from the model.
53. B. H. Hager and R. W. Clayton, in *Mantle Convection*, W. R. Peltier, Ed. (Gordon and Breach, New York, 1989), pp. 657–764.
54. Y. Ricard *et al.*, *J. Geophys. Res.* **98**, 21895 (1993).
55. G. U. Batchelor, *An Introduction to Fluid Mechanics* (Cambridge Univ. Press, Cambridge, 1967).
56. B. L. Isacks, *J. Geophys. Res.* **93**, 3211 (1989); B. M. Sheffels, *Geology* **18**, 807 (1990); P. Baby *et al.*, *Tectonophysics* **205**, 155 (1992).
57. S. P. Grand, *J. Geophys. Res.*, in press.
58. P. G. Silver, R. W. Carlson, P. Olson, *Annu. Rev. Earth Planet. Sci.* **16**, 477 (1988).
59. G. Barruol, thesis, University of Montpellier, Montpellier, France (1993).
60. G. Barruol, P. Silver, A. Vauchez, *Terra Abstr.* **5**, 49 (1993).
61. R. Engdahl, personal communication.
62. R. S. Nerem *et al.*, in preparation.
63. P. Wessel and W. H. F. Smith, *Eos* **72**, 441 (1991).

64. We thank G. Helffrich for revamping the splitting measurement code; S. Schoenecker for help in data processing; J. Gephart and B. Isacks for providing contours of the subducted Nazca plate; S. Nerem and W. Smith for providing geoid data; S. Solomon, B. Hager, K. Fischer, J. P. Morgan, J. Park, S. Sacks, T. Shoberg, W. Smith, and L. Solheim for helpful discussions; two anonymous reviewers for providing useful suggestions; A. Pyrolley and the staff at Institut de Physique du Globe de Paris/GEOSCOPE for providing data for CAY and MBO; J. Dunlap for assistance in manuscript preparation; and J. VanDecar for aid with graphic production. Supported by National Aeronautics and Space Administration grant NAGW-3036.